



Comparison of time transfer of IF-PPP, GIM-PPP, and RIM-PPP

Qile Zhao¹ · Jingyu Guo¹ · Hongming Zuo¹ · Xiaopeng Gong¹ · Wenfei Guo¹ · Shengfeng Gu¹

Received: 25 February 2022 / Accepted: 18 February 2023 / Published online: 5 April 2023
© The Author(s), under exclusive licence to Springer-Verlag GmbH Germany, part of Springer Nature 2023

Abstract

Global navigation satellite system precise point positioning (GNSS PPP) is a technology widely used in precise time and frequency transfer. In this study, we compare PPP time transfer based on ionospheric-free PPP (IF-PPP), undifferenced and uncombined PPP with global ionospheric map constraint (GIM-PPP), and PPP with regional ionospheric map constraint (RIM-PPP). The receiver code bias effect on receiver clock estimates is derived for IF-PPP and GIM-PPP. In the experiment, six GNSS receivers of EUREF Permanent Network (EPN) equipped with the external hydrogen masers (H-MASER) are tested for the day of year (DOY) 009 to 365, 2020, and the regional ionospheric delay modeling estimation is performed with 202 EPN stations for the corresponding period. Then, all the PPP timing solutions are carried out in forward-filtering mode. The results show that the GIM-PPP model and the RIM-PPP mode can be used for PPP one-way timing, with accuracy identical compared to the traditional IF-PPP model. Modified Allan deviation is used to evaluate the time transfer stability. The results show that the short-term frequency stability of the GIM-PPP and RIM-PPP models is significantly better than that of the IF-PPP model, which improves by 20 and 50%, respectively.

Keywords One-way timing · Allan deviation · Regional ionospheric

Introduction

High-precision time transfer is the basis for the time laboratory to establish and maintain standard time scale and time synchronization. With the development of space technology, the precision of time transfer is getting higher and higher. Precise point positioning (PPP) has the advantages of high-precision, wide-area coverage, and convenient data acquisition and processing. In recent years, the time transfer method based on PPP has shown superior performance in terms of precision and coverage, which has made it become one of the most popular Global Navigation Satellite System (GNSS) time transfer methods, and it was applied to the International Atomic Time Scale (TAI) in 2009 (Petit 2009; Petit and Jiang 2007; Yao et al. 2015). With the improvement of precision and timeliness of IGS precise ephemeris and clock products, PPP technology has been applied more in the GNSS time-frequency field. Petit et al. (2011) carried out PPP time transfer experiments based on GPS, and

the results show that the uncertainty u_A of the static PPP time transfer is 0.3ns. Harmegnies et al. (2013) analyzed the time transfer of a GPS single system and GPS + GLONASS combined PPP. The results show that the timing precision of the two schemes is similar, i.e., the precision improvement of GPS + GLONASS multi-system combination timing is rather limited.

Concerning the above studies in PPP timing, the ionospheric-free combination was widely used. Along with the modernization of GPS and GLONASS, as well as the newly launched systems BDS and Galileo (Montenbruck et al. 2017; Yang et al. 2021), multi-frequency GNSS data processing has paved the way for the undifferenced and uncombined PPP (UC-PPP) model (Zhou et al. 2018). Tu et al. (2019) analyze the time transfer performance of IF-PPP and UC-PPP models. The results show that the two models have the same accuracy and stability, and the receiver code bias is very stable that can be predicted for the next day. In undifferenced and uncombined PPP timing, ionospheric delay plays an important role (Rose et al. 2014; Su et al. 2019; Zhang et al. 2020). Ge et al. (2019) compared the time transfer performance of the ionospheric constraint model, the ionospheric correction model, and the ionospheric-free model and pointed out that the accuracy of the ionospheric

✉ Shengfeng Gu
gsf@whu.edu.cn

¹ GNSS Research Center, Wuhan University, 129 Luoyu Road, Wuhan 430079, China

constraint model is better than others. The ionospheric constraint model estimates the ionospheric delay as a parameter constrained by the Global Ionosphere Map (GIM) product, and the ionospheric correction model constraint model directly uses GIM to correct the ionospheric delay. In addition, the standard deviation (STD) values of the ionospheric constraint model time transfer are at the level of 0.5 ns at cutoff elevation angles of 10°, 20°, and 30°. Hexagon Positioning Intelligence (HPI) tested regional ionosphere models (RIM), and the results show that convergence to a 5 cm level can be obtained in several seconds and regional ionospheric products have higher reliability (Jokinen et al. 2018). However, the application of high-precision ionospheric products in time transfer and its in-depth analysis is still left for further study.

We first briefly review the basic principle of PPP time transfer technology, and the emphasis is given to the difference between the ionospheric-free PPP and undifferenced and uncombined PPP; then, the performance of time transfer with different PPP models is analyzed based on six GNSS stations equipped with H-MASERs for over 357 days.

Methods

The undifferenced and uncombined observable of the GNSS pseudorange and carrier phase is generally expressed as (Leick et al. 2015)

$$\left. \begin{aligned} P_{r,f}^s &= \rho_r^s + t_r + \alpha_r^s T_r^s + \beta_f \gamma_r^s I_Z + b_{r,f}^s + \varepsilon_P \\ \phi_{r,f}^s &= \rho_r^s + t_r + \alpha_r^s T_r^s - \beta_f \gamma_r^s I_Z + \lambda_f N_{r,f}^s + \varepsilon_\phi \end{aligned} \right\} \quad (1)$$

where r , s and f are the receiver, satellite and frequency, respectively; $P_{r,f}^s, \phi_{r,f}^s$ are pseudorange and carrier phase from receiver r to satellites s on frequency f in length units, respectively; ρ_r^s denotes the geometric distance between the phase center of the satellite and receiver antennas at the signal transmitting and receiving time, respectively; t_r is the receiver clock bias in units of length; T_r^s is the zenith tropospheric delay that can be converted to slant with the mapping function α ; I_Z denotes the zenith TEC with the frequency and elevation angle dependent factor $\beta_f = \frac{40.3}{f^2} \cdot \text{mf}(e)$; γ_r^s is the ionospheric mapping function; $b_r^s = b_r - b^s$ is the frequency dependent code bias (Li et al. 2011); N_r^s is the float ambiguity in cycle units with the corresponding wave length λ_f ; ε_P and ε_ϕ denote the sum of measurement noise and multipath error for the pseudorange and carrier phase, respectively. In addition, the satellite and receiver antenna phase center offsets (PCOs) and variations (PCVs), earth tides, relativistic effects, and phase wind-up have been corrected with existing models (Kouba 2009).

Ionospheric-free PPP

The IF-PPP model combines observations of different frequencies linearly to eliminate the first-order ionospheric delay term of carrier phase and pseudorange observations. In this model, only receiver coordinates, receiver clock offset, zenith tropospheric delay and ambiguity are estimated (Zhao et al. 2019)

$$\left. \begin{aligned} P_{\text{IF}} &= \rho_r^s + t_r + \alpha_r^s T_r^s + b_{r,\text{IF}}^s + \varepsilon_{\text{IF},P} \\ \phi_{\text{IF}} &= \rho_r^s + t_r + \alpha_r^s T_r^s + \lambda_{\text{IF}} N_{\text{IF}} + \varepsilon_{\text{IF},\phi} \end{aligned} \right\} \quad (2)$$

where the subscript IF represents the ionospheric elimination combination; $P_{\text{IF}}, \phi_{\text{IF}}$ are the IF pseudorange and carrier phase in units of range, respectively, and $P_{\text{IF}} = \gamma_1 P_1 - \gamma_2 P_2$, $\phi_{\text{IF}} = \gamma_1 \phi_1 - \gamma_2 \phi_2$; $\gamma_i = \frac{f_i^2}{f_1^2 - f_2^2}$ ($i = 1, 2$); $b_{r,\text{IF}}^s = \gamma_1 b_{r,1}^s - \gamma_2 b_{r,2}^s$ is the IF code bias; similarly, the definition of the left terms can be obtained by IF combination and (1).

In addition, following the dual-frequency IF combination, the measurement noise of pseudorange and carrier phase is

$$\left. \begin{aligned} \sigma_{\varepsilon_{\text{IF},P}}^2 &= (\gamma_1^2 + \gamma_2^2) \sigma_{\varepsilon_P}^2 \\ \sigma_{\varepsilon_{\text{IF},\phi}}^2 &= (\gamma_1^2 + \gamma_2^2) \sigma_{\varepsilon_\phi}^2 \end{aligned} \right\} \quad (3)$$

where σ^2 is the variance of the corresponding measurement noise. By substituting f_1 and f_2 into (3), it is derived that $\sigma_{\varepsilon_{\text{IF},P}}^2 \approx 8.87 \varepsilon_P$ and $\sigma_{\varepsilon_{\text{IF},\phi}}^2 \approx 8.87 \varepsilon_\phi$; thus, the noise of IF combination is much larger than that of the undifferenced and uncombined observable.

Ionospheric hardware delay in pseudorange observations will be fully absorbed by receiver clock offset through IF combination

$$t_{r,\text{IF}} = t_r + b_{r,\text{IF}} = t_r + \gamma_1 b_{r,1} - \gamma_2 b_{r,2} \quad (4)$$

where the definition of γ and b_r can be obtained by (1).

Undifferenced and uncombined PPP

Although the IF combination can eliminate the influence of the first-order term of the ionospheric, the combined observation noise would be amplified in (3). To solve this problem, the undifferenced and uncombined model is proposed in which the individual signal of each frequency is treated as an independent observation. And the basic model is written as (1). One of the main features of the undifferenced and uncombined model is that the ionospheric delay should be estimated along with the geometry parameters. Traditionally, the LOS (line of sight) ionospheric delay is treated as an independent parameter, whereas in this study, the ionospheric parameterization method DESIGN (deterministic plus stochastic

ionospheric delay modeling for GNSS) is applied in the undifferenced and uncombined model (Lou et al. 2016; Shi et al. 2012)

$$\left. \begin{aligned} I_Z &= a_0 + a_1 d_L + a_2 d_L^2 + a_3 d_B + a_4 d_B^2 + r_r^s \\ I_{\text{corr}} &= a_0 + a_1 d_L + a_2 d_L^2 + a_3 d_B + a_4 d_B^2 + r_r^s + \varepsilon_I \end{aligned} \right\} \quad (5)$$

where I_Z is the zenith ionospheric delay from receiver to satellite, I_{corr} is the ionosphere delay correction from, e.g., GIM or a regional high-precision ionospheric delay model (RIM), as in this study; $a_i (i = 0, 1, 2, 3, 4)$ are the coefficients that describe the deterministic behavior of ionospheric delay; r_r^s is the residual ionospheric effect for each satellite that describes the stochastic behavior of ionospheric delay; d_L , d_B is the longitude and latitude difference between the Ionospheric Pierce Point (IPP) and the approximate location of the station, respectively; ε_I is the ionospheric parameter fitting estimation noise.

In addition, to eliminate the linear dependence of receiver clock offset and code bias, we have the following assumption

$$t_{r,UC} = t_r + b_{r,1} \quad (6)$$

where $t_{r,UC}$ is the receiver clock solved by the undifferenced and uncombined PPP model.

By substituting (5) and (6) into (1), the dual-frequency undifferenced and uncombined PPP model based on DESIGN is written as

$$\left. \begin{aligned} P_{r,1}^s &= \rho_r^s + t_{r,UC} + \alpha_r^s T_r^s + \beta_1 \gamma_r^s (a_0 + a_1 d_L + a_2 d_L^2 + a_3 d_B + a_4 d_B^2 + r_r^s) + b^s + \varepsilon_P \\ P_{r,2}^s &= \rho_r^s + t_{r,UC} - b_{r,12} + \alpha_r^s T_r^s + \beta_2 \gamma_r^s (a_0 + a_1 d_L + a_2 d_L^2 + a_3 d_B + a_4 d_B^2 + r_r^s) + b^s + \varepsilon_P \\ \phi_{r,1}^s &= \rho_r^s + t_{r,UC} + \alpha_r^s T_r^s - \beta_1 \gamma_r^s (a_0 + a_1 d_L + a_2 d_L^2 + a_3 d_B + a_4 d_B^2 + r_r^s) + \lambda_1 N_{r,1}^s + \varepsilon_\phi \\ \phi_{r,2}^s &= \rho_r^s + t_{r,UC} + \alpha_r^s T_r^s - \beta_2 \gamma_r^s (a_0 + a_1 d_L + a_2 d_L^2 + a_3 d_B + a_4 d_B^2 + r_r^s) + \lambda_1 N_{r,2}^s + \varepsilon_\phi \\ I_{\text{corr}} &= a_0 + a_1 d_L + a_2 d_L^2 + a_3 d_B + a_4 d_B^2 + r_r^s + \varepsilon_I \end{aligned} \right\} \quad (7)$$

where parameters definitions can be obtained from (1) and (5); b^s is the satellite code bias that can be corrected with IGS products; concerning the receiver code bias, though $b_{r,1}$ is absorbed by the receiver clock as (6), the code bias on the second frequency is $b_{r,12} = b_{r,1} - b_{r,2}$ to make model (7) hold. $b_{r,12}$ is usually known as differential code bias (DCB) and usually rather stable.

Recall (4) and (6), the difference of receiver clock between IF-PPP and undifferenced and uncombined PPP can be derived as

$$t_{r,IF} = t_{r,UC} + \gamma_2 b_{r,12} \quad (8)$$

where the bias is due to the different parameterization and rank deficiency elimination strategy are used for IF-PPP and undifferenced and uncombined PPP.

Assessment of clock stability with PPP

Considering the linear relationship between the receiver and the satellite clock, the extensive constraint on the satellite clock is (Yang et al. 2019) :

$$\sum_{s=1}^k t^{s,\text{sys}} = 0 \quad (9)$$

where $t^{s,\text{sys}}$ is satellite clock belonging to $\text{sys} \in (GRCE)$. In addition, considering the linear relationship between the satellite clock and carrier phase ambiguity, as well as the additional bias generated by satellites in the same system, the satellite clock estimate can be written:

$$\hat{t}^{s,\text{sys}} = t^{s,\text{sys}} - t^{0,\text{sys}} + \varepsilon^{s,\text{sys}} \quad (10)$$

where $t^{0,\text{sys}}$ is the reference clock offset caused by the linear relationship among the system satellite clock, receiver clock, and ambiguities; $\varepsilon^{s,\text{sys}}$ is the estimation noise.

Considering the reference clock in PPP, $t^{0,\text{sys}}$, would be absorbed by the receiver clock,

$$\hat{t}_r^{\text{sys}} = t_r^{\text{sys}} - t^{0,\text{sys}} + \varepsilon_r \quad (11)$$

where t_r^{sys} is the receiver clock belonging to sys and ε_r is the estimation noise, then the time difference between two receivers using the same satellite system:

$$\Delta \hat{t}_{r_i, r_j}^{\text{sys}} = \hat{t}_{r_i}^{\text{sys}} - \hat{t}_{r_j}^{\text{sys}} = t_{r_i}^{\text{sys}} - t_{r_j}^{\text{sys}} + \varepsilon_{r_i} - \varepsilon_{r_j} (i \neq j) \quad (12)$$

The symbols meaning on the right of the equal sign are the same as (14).

The overlapping Allan deviation is used to evaluate the stability of the receiver clock. Based on (11) and (12), considering that the receivers used in this experiment are equipped with the external H-MASER, the effect of t_r^{sys} can be ignored, then we can obtain:

Table 1 Specification and ADEV (s)

Avg	iMaser3000	VCH-1003M	MHM-2010	pHMaser 1008	CH1-95
1	6.33×10^{-12}	1.5×10^{-13}	3.06×10^{-14}	5×10^{-13}	1.2×10^{-13}
10	1.29×10^{-14}	2.5×10^{-14}		2×10^{-13}	2.5×10^{-14}
100	3.11×10^{-15}	6×10^{-14}	6.04×10^{-15}	5×10^{-14}	4.5×10^{-15}
1000	8.71×10^{-16}		2.83×10^{-15}		1.5×10^{-15}
1 h		2×10^{-15}		9×10^{-15}	1.3×10^{-15}
10,000	3.15×10^{-16}		3.48×10^{-15}		3.5×10^{-16}
1 day		5×10^{-16}		4×10^{-15}	5×10^{-16}

$$\left. \begin{aligned} \delta_y^2(\tau, \hat{t}_r^{\text{sys}}) &\approx \delta_y^2(\tau, t^{0,\text{sys}}) + \delta_y^2(\tau, \epsilon_r) \\ \delta_y^2(\tau, \Delta \hat{t}_{r_1, r_j}^{\text{sys}}) &= \delta_y^2(\tau, \hat{t}_{r_i}^{\text{sys}}) + \delta_y^2(\tau, \hat{t}_{r_j}^{\text{sys}}) \approx 2\delta_y^2(\tau, \epsilon_r) (i \neq j) \end{aligned} \right\} \quad (13)$$

the symbolic meaning on the right of the equal sign can be found from (10) to (12).

When tested with k receivers, we can get k receivers and $k - 1$ time synchronization overlapping Allan deviation. We can use the following model to obtain $\delta^2(\tau, \epsilon_r)$:

$$\begin{pmatrix} \delta_y^2(\tau, \hat{t}_{r_1}^{\text{sys}}) \\ \vdots \\ \delta_y^2(\tau, \hat{t}_{r_k}^{\text{sys}}) \\ \delta_y^2(\tau, \Delta \hat{t}_{r_1, r_2}^{\text{sys}}) \\ \vdots \\ \delta_y^2(\tau, \Delta \hat{t}_{r_1, r_k}^{\text{sys}}) \end{pmatrix} = \begin{pmatrix} \mathbf{u}_k & \mathbf{u}_k \\ 2\mathbf{u}_{k-1} & \mathbf{z}_{k-1} \end{pmatrix} \begin{pmatrix} \delta_y^2(\tau, \epsilon_r) \\ \delta_y^2(\tau, t^0) \end{pmatrix} \quad (14)$$

where $\mathbf{u}_k = (1 \ 1 \ \dots \ 1)^T$ is a $k \times 1$ vector with one entry; $\mathbf{z}_k = (0, 0 \dots 0)^T$ is a $k \times 1$ vector with zero entries.

Ionospheric modeling

Based on (5) and (7), we can obtain the vertical TEC of the ionospheric pierce point (IPP) and convert it to slant TEC (STEC) by the ionospheric mapping function γ . Then, the ionospheric variations can be fitted by the Quasi-4-Dimension Ionospheric Modeling (Q4DIM) (Gu et al. 2022). For the Q4DIM users, the ionospheric delay corrections are obtained as:

$$\text{STEC}_r^s = I_o^s + r_r^s \quad (15)$$

where I_o^s is ionospheric delay deterministic part; it can be either interpolated from grids or calculated with the Spherical Harmonic Function (SHF) of GIM with a mapping function. r_r^s is obtained according to the key values in the Q4DIM map.

Experimental data and processing strategies

To assess the performance of PPP time transfer, all the above-mentioned algorithms, i.e., IF-PPP, undifferenced and uncombined PPP, RIM products are realized with the FUSING (FUSing IN GNSS) software. Up to now, FUSING is capable of real-time multi-GNSS precise POD, satellite clock estimation, atmosphere modeling, and multi-sensor navigation. (Gong et al. 2018; Shi et al 2019; Luo et al. 2020; Gu et al. 2021).

Data and strategy

The experiment is carried out with six GNSS stations of EUREF Permanent Network (EPN), BRUX, OP71, PTBB, ROAG, SPT0, and WAB2. These stations are involved in Bureau International des Poids et Mesures (BIPM) TAI maintenance and are equipped with H-MASER (iMaser 3000 active hydrogen maser standards for BRUX and OP71; VCH-1003M active hydrogen maser standards for PTBB; MHM-2010 active H-MASER standards for ROAG; CH1-95 hydrogen maser standard for SPT0; pHMaser 1008 passive hydrogen maser standards for WAB2;), and the specifications of these clocks are given in Table 1; thus, the stability of the receiver clock frequency standard itself is relatively negligible in PPP clock estimation noise evaluation. In addition, 202 stations are selected for the regional ionospheric model (Wang et al. 2021; Geng et al. 2021). To extract regional ionospheric products, the spatial and temporal resolution of bins of $5^\circ \times 3^\circ$ and 1 minute, respectively, have been selected. The observation is collected for DOY (day of year) 009 to 365, 2020 with an interval of 30s. Though the signals of BDS+GPS+Galileo+GLONASS are tracked by these stations, only the receiver clock of the GPS is used since the receiver clocks of different systems are estimated as individual parameters. Precise orbit and clock products are provided by the Helmholtz-Centre Potsdam-German

Table 2 Summaries of the station information

Station	Receiver	Antenna	Clock
BRUX	SEPT POLARX5TR	AVRINGANT_DM	UTC (ORB)
OP71	SEPT POLARX4TR	LEIAR25.R4	UTC (OP)
PTBB	SEPT POLARX5TR	LEIAR25.R4	UTC (PTB)
ROAG	SEPT POLARX5TR	LEIAR25.R4	UTC (ROA)
SPT0	SEPT POLARX5TR	TRM59800.00	UTC (SP)
WAB2	SEPT POLARX5TR	SEPCHOKE_B3E6	UCT (CH)

Centre for Geoscience Research (GFZ), which are calculated from data from the Multi-GNSS Experiment (MGEX) in the global region (Montenbruck et al. 2017). And the final precise orbit and clock products of GFZ, i.e., GBM provide multi-system satellite products, and the satellite clock product is consistent with the ionospheric-free combination of L1 and L2. Table 2 presents the details of the stations. In addition, Table 3 lists the details of PPP processing strategies; the receiver DCB uses the smooth convergence value of the previous day as a constraint. Note that the undifferenced and uncombined PPP in this work is constrained by GIM and RIM products, so we name them GIM-PPP and RIM-PPP, respectively. Except for the orbit and clock, regional ionospheric products and PPP are processed in forward-filtering decoding mode with Square Root Information Filter (SRIF).

Performance analysis

In the following analysis, we first demonstrate the precision of regional ionospheric products. Then, the performance of GNSS timing based on a different algorithm, i.e., IF-PPP, GIM-PPP, and RIM-PPP is analyzed in terms of Allan deviation.

Efficiency of regional ionospheric product and ambiguity resolution

High-precision ionospheric delay correction is the key to improving the convergence speed and positioning accuracy of the undifferenced and uncombined PPP model (Song et al. 2021). The distribution of these base stations is shown in Fig. 1. In order to evaluate the precision of the regional ionospheric High-precision products, the post-processed ionospheric delay of the six laboratories with maser-equipped GNSS receivers with fixed coordinates was used as the reference.

Fig. 2 shows the time series of the ionosphere delay differences at the zenith between the regional ionospheric

product and the reference value within one day, with a cutoff angle of 10°. The result of BRUX is selected arbitrarily as an example. We can see that the ionosphere delay differences are almost all less than 0.2 m. In addition, Fig. 3 presents the average RMS of GPS satellites for 357 consecutive days at BRUX, OP71, PTBB, ROAG, SPT0, and WAB2. The ionospheric delays in the zenith direction at the stations are obviously better than 0.10 m. Comparing the RMS of the RIM product at day and night, it can be seen that the accuracy of the RIM products at day and night is comparable, which is highly significant for the RIM-PPP model.

Fig. 4 presents the percentage of available satellites at the cutoff elevation angle of 10° for BRUX, OP71, PTBB, ROAG, SPT0, and WAB2. As presented, we usually have 6 to 11 satellites available; the average number of available satellites is (8.76, 8.38, 8.62, 8.53, 8.95, 8.48), respectively. This is acceptable for PPP time transfer. In addition, the data integrity rates of observations during the experiment are (99.90%, 99.99%, 99.74%, 99.90%, 99.99%, 99.63%), and the data integrity rate of all stations is better than 99.50%.

PPP one-way timing analysis

Figure 5 shows the clock series of the solution IF-PPP (black), GIM-PPP (red), and RIM-PPP (blue) for 357 consecutive days of the experimental period. As presented, there is a bias between IF-PPP and GIM-PPP/ RIM-PPP due to the receiver code bias in Fig. 6. Note that BRUX changed the receiver on DOY 56, 2020 and SPT0 changed the antenna on DOY 226, 2020 (<https://www.igs.org/>). Overall, the clocks of these stations are rather stable with an amplitude of 2.5 ns intraday and 8 ns in a year, as the high-quality atomic frequency standards data. The fluctuation in the series was mainly due to the noise in the satellite clock datum and PPP processing. As the same satellite clock product is used, the performance comparison revealed the noise of one-way timing with different PPP algorithms. The series suggests that, overall, the PPP noise of different algorithms is similar to each other. The receiver code bias between P1 and P2 is plotted in Fig. 6 for GIM-PPP, and RIM-PPP, respectively. As we can see, these biases are rather stable, with an amplitude

of 1 ns in a year, and have similar performance for different stations. In addition, we note that there are similar fluctuations in the receiver P1-P2 code bias estimated value series for different stations, and the STD of the receiver P1-P2 code bias series is slightly larger for the RIM-PPP model than for the GIM-PPP model. With (7), this is mainly due to the strong correlation between ionospheric delay and DCB. Thus, the fluctuation of the P1-P2 DCB estimation sequence is similar for different stations, and the STD of the P1-P2 DCB series for the RIM-PPP model is larger than that of the GIM-PPP model due to the higher accuracy of RIM and the stronger constraint on DCB.

With (8), the receiver estimated clock bias for IF-PPP and UC-PPP models should be zero. Table 4 shows the 357d average difference between the GIM-PPP and RIM-PPP models compared to the IF-PPP model at different stations during the test period of the experiment. As shown in Table, the receiver estimated clock bias for the GIM-PPP and the RIM-PPP models is extremely small compared to the IF-PPP model, in addition, we note that the deviation between the RIM-PPP model and the IF-PPP model is slightly larger for the ROAG and WAB2 stations than for the other stations. According to Fig. 3, it can be seen that the ionospheric accuracy of the two stations is slightly worse than that of the other stations and fluctuates considerably over the year, which affects the accuracy of the PPP one-way timing.

Stability of PPP time transfer

To assess the stability of PPP time transfer, Fig. 7 presents the 357d average overlapping Allan deviations of PPP one-way timing, i.e., $\delta_y^2(\tau, \hat{t}_r^{yy})$ in (13), of BRUX, OP71, PTBB, ROAG, SPT0, and WAB2 at different time intervals with

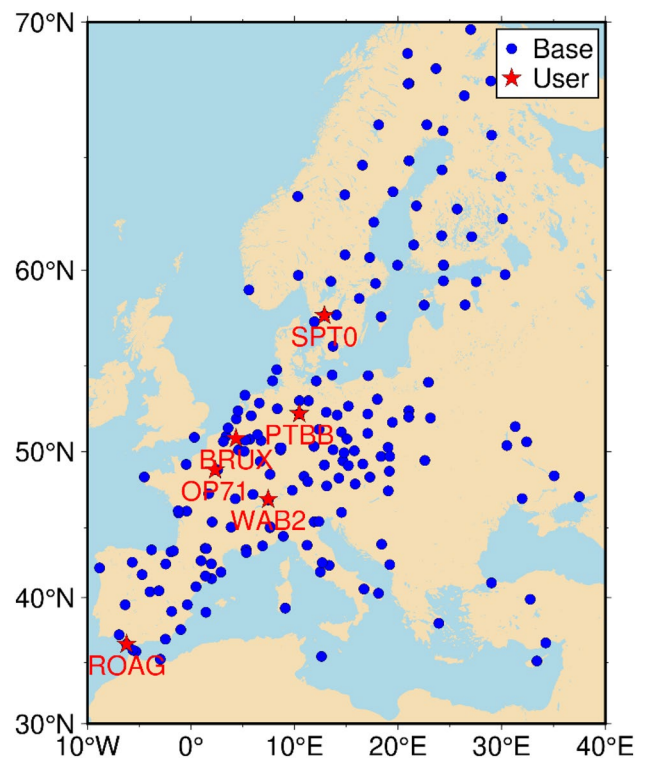


Fig. 1 Geographical distribution of 202 selected GNSS tracking stations in blue for ionospheric delay modeling, and six time laboratory stations in red for PPP timing

IF-PPP, GIM-PPP, and RIM-PPP, respectively. As shown in this figure, RIM-PPP presents the best result for stability. This is most likely due to the fast convergence of RIM-PPP when compared to IF-PPP and GIM-PPP, and regional

Table 3 Details of PPP processing strategy

Item	IF-PPP	GIM-PPP	RIM-PPP
Signals	GPS: L1/L2		
Receiver types	Table 2		
Ephemeris	GBM		
Cutoff angle	10°		
Sample Interval	30 s		
Ionosphere	Dual-frequency combination	DESIGN with GIM as a priori correction	DESIGN with the regional ionospheric delay model as a priori correction
Troposphere	GPT2		
PCO and PCV	IGS_14		
DCB		Daily constant	
Continuity	Restart at 00:00 GPST		
Coordinate	Estimated as fixed in static mode		
Clock Noise	White noise with $E(\sigma^2) = 100$ ns		
Ambiguity	Float		
Solution	Square root information filter		
Software	FUSING		

Fig. 2 Time series of ionospheric delay differences at the zenith of satellite G01 to G32 between regional ionospheric products and post-processing model on frequency L1 for BRUX at DOY 010, 2020.

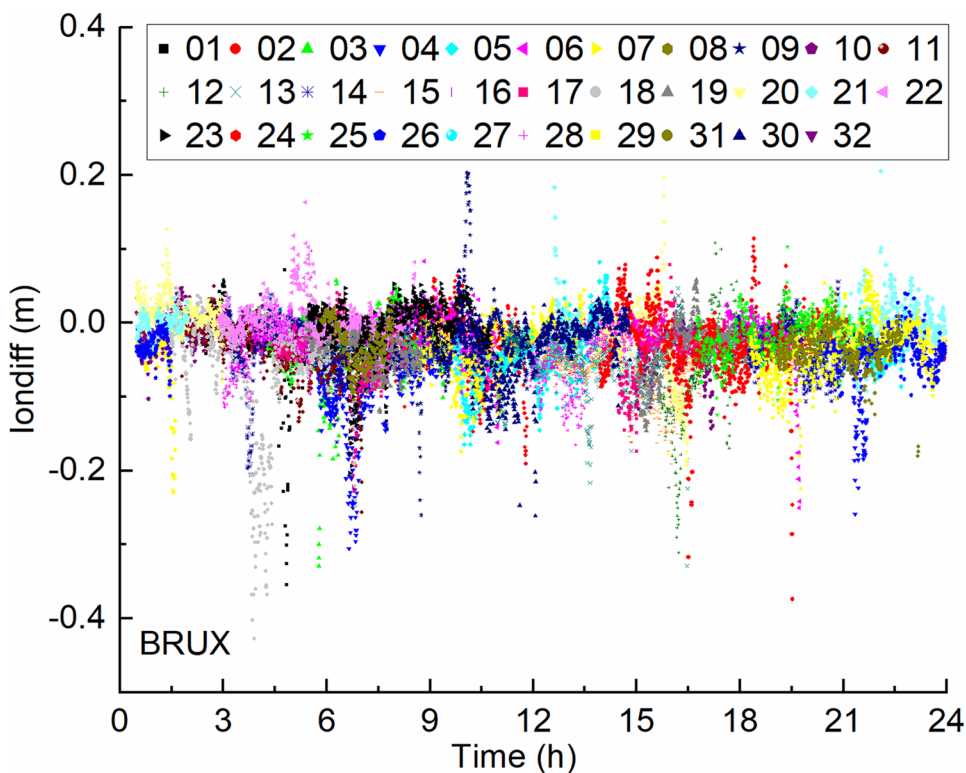


Fig. 3 Day and night RMS of the ionospheric delay differences at the zenith between regional ionospheric products and post-processing value on frequency L1 from DOY 009 to 365, 2020 for BRUX, OP71, PTBB, ROAG, SPT0, and WAB2, respectively

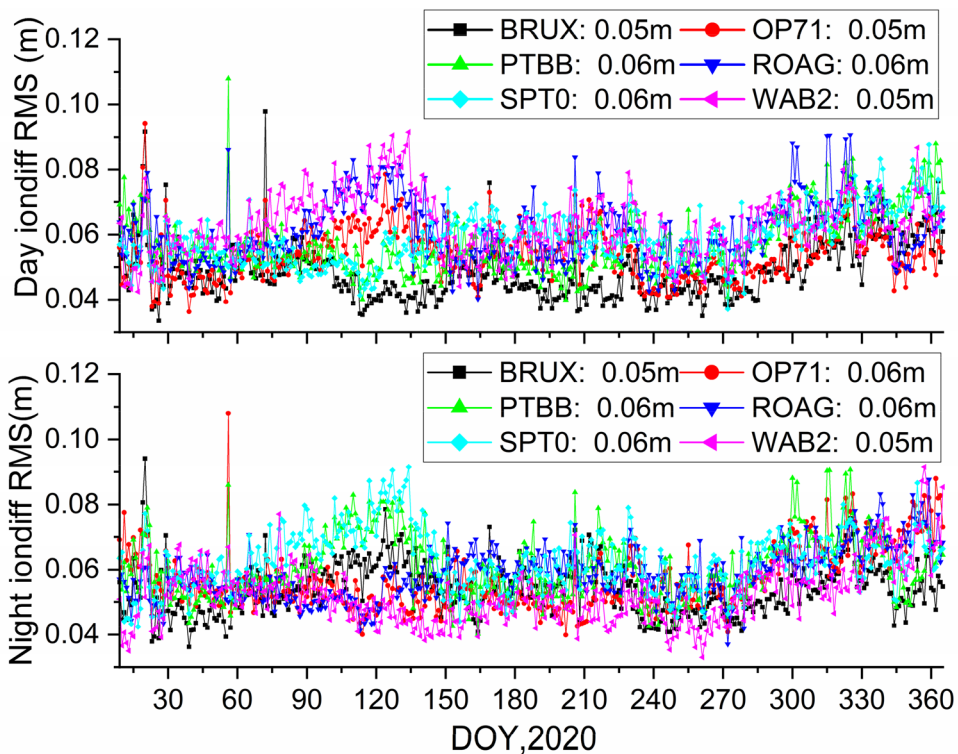


Fig. 4 Percentage of available satellites for BRUX, OP71, PTBB, ROAG, SPT0, and WAB2, respectively

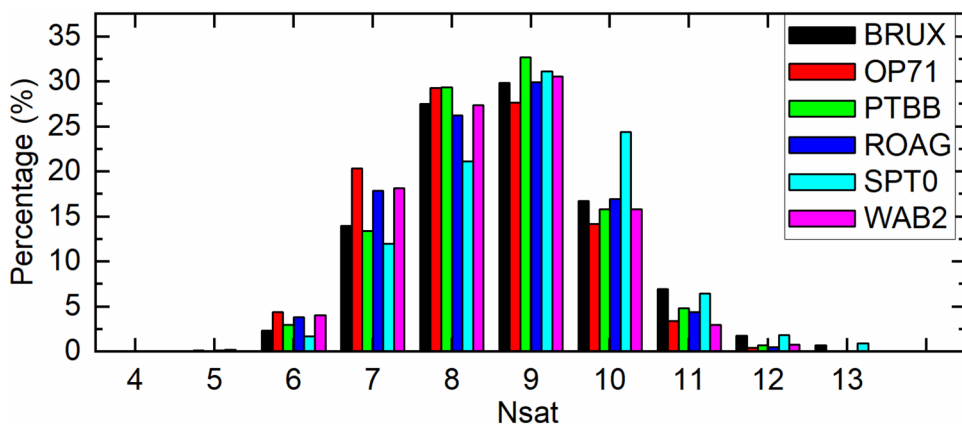


Fig. 5 Receiver clock series of IF-PPP, GIM-PPP, and RIM-PPP model timing from DOY 009 to 365, 2020 for BRUX, OP71, PTBB, ROAG, SPT0, and WAB2, respectively.

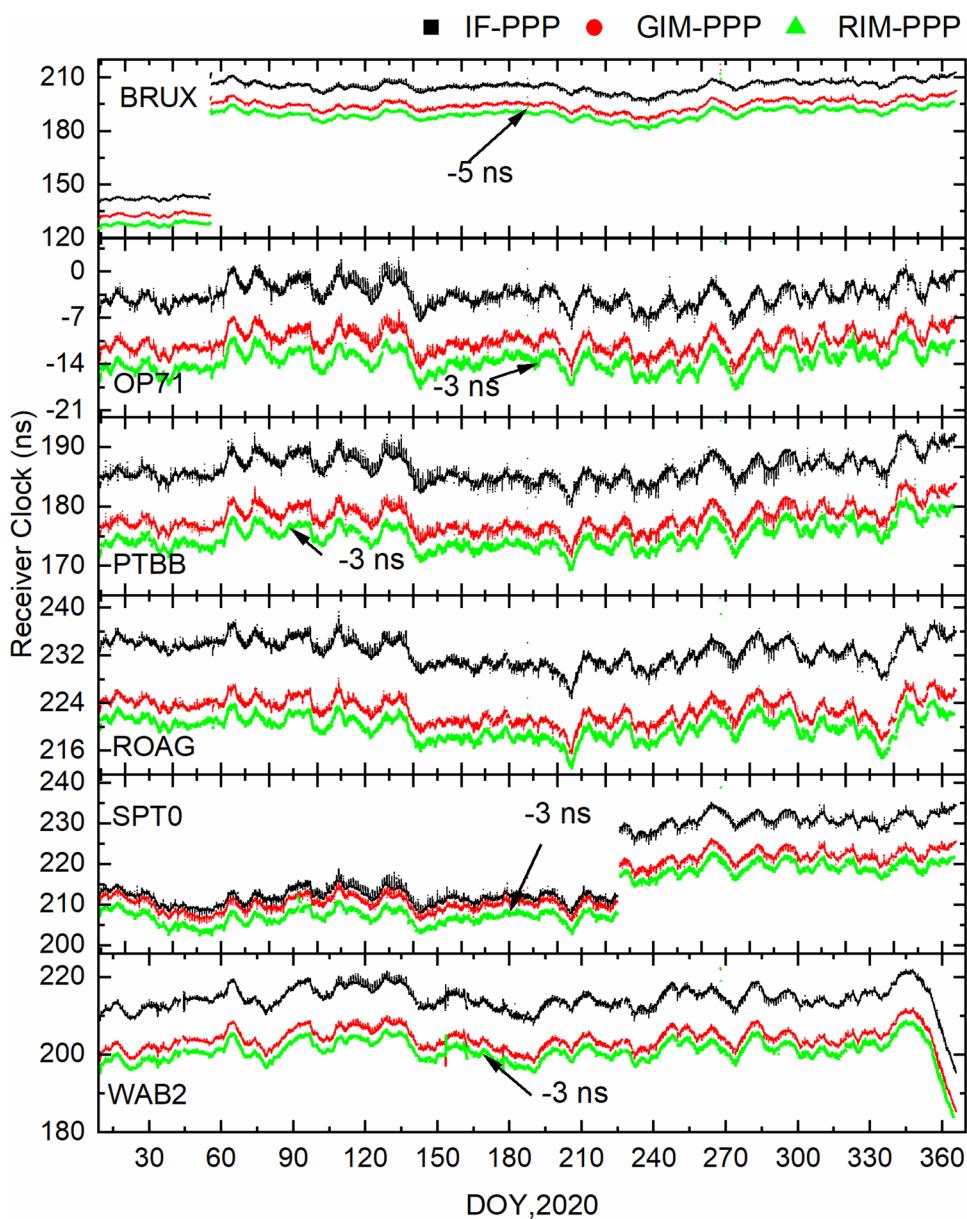


Fig. 6 Series of the receiver P1P2 DCB estimated values over DOY 009 to 365, 2020 with GIM-PPP model in red and RIM-PPP model in green for BRUX, OP71, PTBB, ROAG, SPT0, and WAB2, respectively.

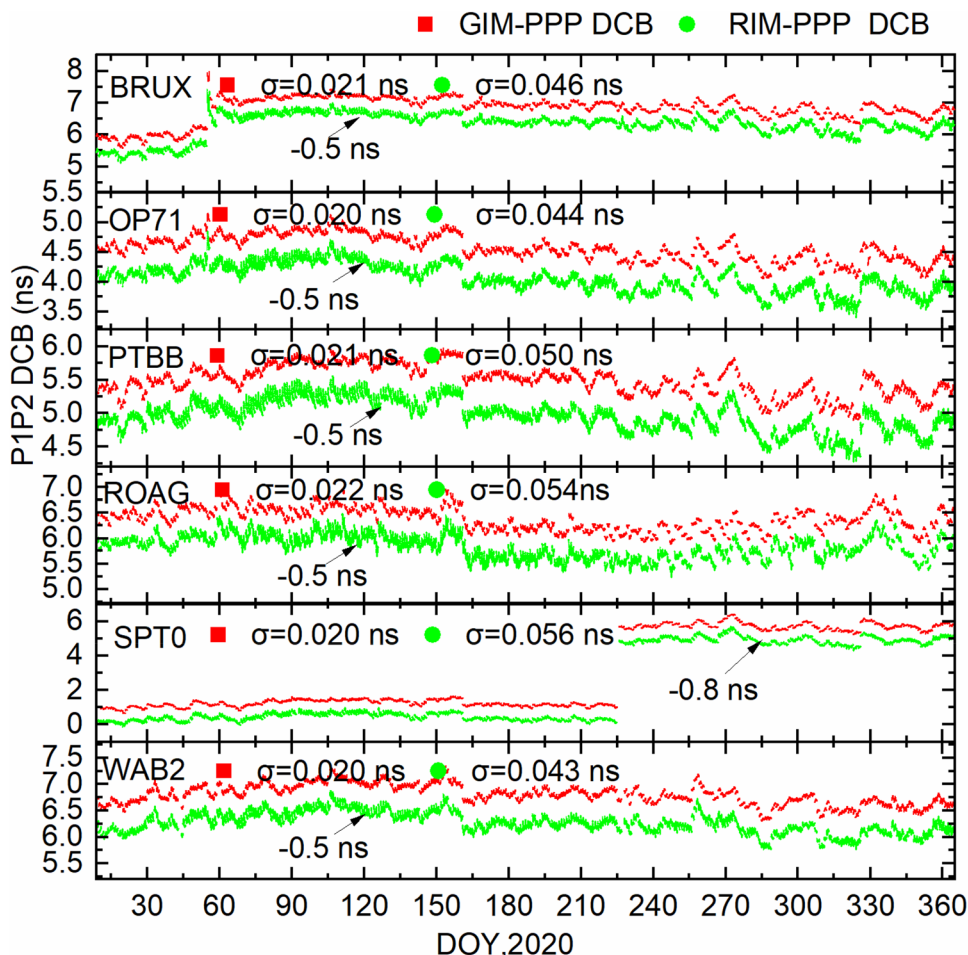


Table 4 Model biases of GIM-PPP and RIM-PPP compared to IF-PPP model for one-way timing (units: ns)

Station	GIM-PPP	RIM-PPP
BRUX	-0.03	-0.02
OP71	0.04	0.06
PTBB	-0.07	-0.07
ROAG	-0.07	-0.13
SPT0	-0.04	0.01
WAB2	-0.06	-0.10

ionospheric products are more stable. The results of GIM-PPP are slightly better than that of IF-PPP.

With (14), we can derive the Allan deviations of data processing noise $\delta_y^2(\tau, \epsilon_r)$ for different PPP solutions. And the results are presented in Fig. 8. As we can see, the Allan deviations of estimated noise in IF-PPP, GIM-PPP, and RIM-PPP models have a similar trend. Because the IF-PPP model uses an unsmoothed linear combination of observations, the overall Allan deviation of the IF-PPP model is

worse than that of the other solutions. In addition, since RIM-PPP uses high-precision regional ionospheric products, its stability is obviously better than that of the IF-PPP and GIM-PPP models.

Conclusions

This study assesses the PPP time transfer performance with different solutions, i.e., IF-PPP, GIM-PPP, and RIM-PPP in simulated real-time mode. The experiment is carried out with EPN observations from six maser-equipped laboratory stations and GBM products from DOY 009 to 365, 2020. To enable the RIM-PPP solution, 202 stations of EPN are collected for the estimation of the regional ionospheric model.

For PPP one-way timing, the GIM-PPP and the RIM-PPP models have comparable accuracy compared to the IF-PPP model. In terms of time transfer stability, we separated the PPP estimation noise for the evaluation and the results show

Fig. 7 Modified Allan deviations of IF-PPP, GIM-PPP, and RIM-PPP model receiver clock series from DOY 009 to 365, 2020 for BRUX, OP71, PTBB, SPT0 and WAB2, respectively

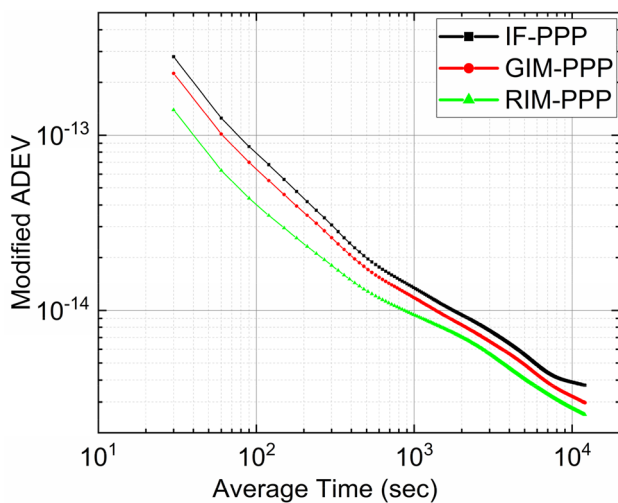
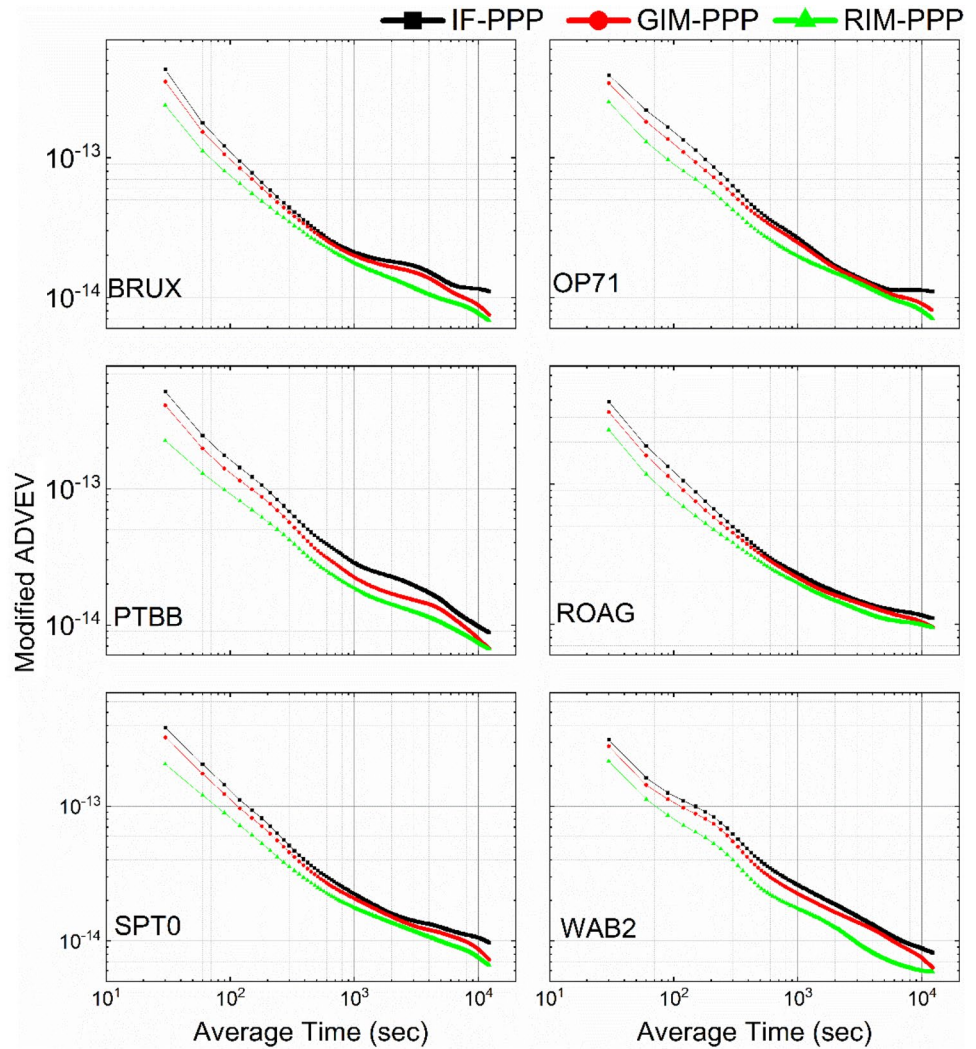


Fig. 8 Modified Allan deviations of PPP data processing noise with IF-PPP, GIM-PPP, and RIM-PPP model

that both the GIM-PPP and RIM-PPP models show improvements over the traditional IF-PPP model. The short-term stabilities of GIM-PPP and RIM-PPP models are significantly improved; the improvement is about 20% and 50%, respectively. The long-term stabilities for GIM-PPP and RIM-PPP are improved by about 17 and 29%, respectively.

Acknowledgments This study was sponsored by the National Natural Science Foundation of China (42174029, 41904016). The authors thank IGS for data provision.

Data availability statement We would like to acknowledge the efforts of the IGS MGEX campaign in providing multi-GNSS data and products. The observation data are available from EUREF Permanent Network (<https://www.epncb.oma.be>), and the GBM products are available from GFZ (<ftp://ftp.gfz-potsdam.de/GNSS/products/mgex/>).

References

- Jokinen A, Ellum C, Webster I, Shanmugam S, Sheridan K (2018) NovAtel CORRECT with precise point positioning (PPP): recent developments. In: Proc. ION GNSS 2018, Institute of Navigation, Miami, Florida, September 24–28, pp 1866–1882. <https://doi.org/10.33012/2018.15824>
- Geng J, Yang S, Guo J (2021) Assessing IGS GPS/Galileo/BDS-2/BDS-3 phase bias products with PRIDE IPPP. *Satell Navig* 2(1):1–15. <https://doi.org/10.1186/s43020-021-00049-9>
- Ge Y, Zhou F, Dai P, Qin W, Wang S, Yang X (2019) Precise point positioning time transfer with multi-GNSS single-frequency observations. *Measurement* 146:628–642. <https://doi.org/10.1016/j.measurement.2019.07.009>
- Gong X, Gu S, Lou Y, Zheng F, Ge M, Liu J (2018) An efficient solution of real-time data processing for multi-GNSS network. *J Geodesy* 92(7):797–809. <https://doi.org/10.1007/s00190-017-1095-x>
- Gu S, Dai C, Fang W, Zheng F, Wang Y, Zhang Q, Lou Y, Niu X (2021) Multi-GNSS PPP/INS tightly coupled integration with atmospheric augmentation and its application in urban vehicle navigation. *J Geodesy* 95(6):64. <https://doi.org/10.1007/s00190-021-01514-8>
- Gu S, Gan C, He C, Lyu H, Hernandez-Pajares M, Lou Y, Geng J, Zhao Q (2022) Quasi-4-dimension ionospheric modeling and its application in PPP. *Satell Navig* 3(1):24. <https://doi.org/10.1186/s43020-022-00085-z>
- Harmegnies A, Defraigne P, Petit G (2013) Combining GPS and GLO-NASS in all-in-view for time transfer. *Metrologia* 50(3):277. <https://doi.org/10.1088/0026-1394/50/3/277>
- Kouba J (2009) A guide to using International GNSS Service (IGS) products. Geodetic Survey Division Natural Resources Canada. Available via IGS. <http://acc.igs.org/UsingIGSProductsVer21.pdf>
- Leick A, Rapoport L, Tatarnikov D (2015) Satellite Systems. In: GPS satellite surveying, 4th edn. Wiley, Hoboken, pp 207–255
- Li X, Zhang X, Ge M (2011) Regional reference network augmented precise point positioning for instantaneous ambiguity resolution. *J Geodesy* 85(3):151–158. <https://doi.org/10.1007/s00190-010-0424-0>
- Lou Y, Zheng F, Gu S, Wang C, Guo H, Feng Y (2016) Multi-GNSS precise point positioning with raw single-frequency and dual-frequency measurement models. *GPS Solut* 20(4):849–862. <https://doi.org/10.1007/s10291-015-0495-8>
- Luo X, Gu S, Lou Y, Cai L, Liu Z (2020) Amplitude scintillation index derived from C/N0 measurements released by common geodetic GNSS receivers operating at 1 Hz. *J Geodesy* 94(2):27. <https://doi.org/10.1007/s00190-020-01359-7>
- Montenbruck O et al (2017) The multi-GNSS experiment (MGEX) of the International GNSS Service (IGS)—achievements, prospects and challenges. *Adv Space Res* 59(7):1671–1697. <https://doi.org/10.1016/j.asr.2017.01.011>
- Petit G (2009) The TAIPPP pilot experiment. In: The 2009 IEEE international frequency control symposium joint with the 22nd European frequency and time forum. IEEE, Besancon, pp 116–119. <https://doi.org/10.1109/freq.2009.5168153>
- Petit G, Harmegnies A, Mercier F, Perosanz F, Loyer S (2011) The time stability of PPP links for TAI. In: The 2011 joint conference of the IEEE international frequency control and the European frequency and time forum (FCS) proceedings. IEEE, San Francisco, pp 1–5. <https://doi.org/10.1109/FCS.2011.5977299>
- Petit G, Jiang Z (2007) Precise point positioning for TAI computation. In: 2007 IEEE international frequency control symposium joint with the 21st European frequency and time forum. IEEE, Geneva, pp 395–398. <https://doi.org/10.1109/freq.2007.4319104>
- Rose JA, Watson RJ, Allain DJ, Mitchell CN (2014) Ionospheric corrections for GPS time transfer. *Radio Sci* 49(3):196–206. <https://doi.org/10.1002/2013rs005212>
- Shi C, Gu S, Lou Y, Ge M (2012) An improved approach to model ionospheric delays for single-frequency Precise Point Positioning. *Adv Sp Res* 49(12):1698–1708. <https://doi.org/10.1016/j.asr.2012.03.016>
- Shi C, Guo S, Gu S, Yang X, Gong X, Deng Z, Ge M, Schuh H (2019) Multi-GNSS satellite clock estimation constrained with oscillator noise model in the existence of data discontinuity. *J Geodesy* 93(4):515–528. <https://doi.org/10.1007/s00190-018-1178-3>
- Song W, He C, Gu S (2021) Performance analysis of ionospheric enhanced PPP-RTK in different latitudes. *Geomat Inf Sci Wuhan Univer* 46(12):1832–1842. <https://doi.org/10.13203/j.whugis20210243>
- Su K, Jin S, Hoque MM (2019) Evaluation of ionospheric delay effects on multi-GNSS positioning performance. *Remote Sens* 11(2):171. <https://doi.org/10.3390/rs11020171>
- Tu R, Zhang P, Zhang R, Liu J, Lu X (2019) Modeling and performance analysis of precise time transfer based on BDS triple-frequency un-combined observations. *J Geodesy* 93(6):837–847. <https://doi.org/10.1007/s00190-018-1206-3>
- Wang J, Zhang Q, Huang G (2021) Estimation of fractional cycle bias for GPS/ BDS-2/ Galileo based on international GNSS monitoring and assessment system observations using the uncombined PPP model. *Satell Navig* 2(1):1–11. <https://doi.org/10.1186/s43020-021-00039-x>
- Yang X, Gu S, Gong X, Song W, Lou Y, Liu J (2019) Regional BDS satellite clock estimation with triple-frequency ambiguity resolution based on undifferenced observation. *GPS Solut*. <https://doi.org/10.1007/s10291-019-0828-0>
- Yang Y et al (2021) Featured services and performance of BDS-3. *Sci Bull* 66(20):2135–2143. <https://doi.org/10.1016/j.scib.2021.06.013>
- Yao J, Skakun I, Jiang Z, Levine J (2015) A detailed comparison of two continuous GPS carrier-phase time transfer techniques. *Metrologia* 52(5):666–676. <https://doi.org/10.1088/0026-1394/52/5/666>
- Zhang J, Gao J, Yu B, Sheng C, Gan X (2020) Research on remote GPS common-view precise time transfer based on different ionosphere disturbances. *Sensors* 20(8):2290. <https://doi.org/10.3390/s20082290>
- Zhao Q, Wang Y, Gu S, Zheng F, Shi C, Ge M, Schuh H (2019) Refining ionospheric delay modeling for undifferenced and uncombined GNSS data processing. *J Geodesy* 93(4):545–560. <https://doi.org/10.1007/s00190-018-1180-9>
- Zhou F, Dong D, Li W, Jiang X, Wickert J, Schuh H (2018) GAMP: an open-source software of multi-GNSS precise point positioning using undifferenced and uncombined observations. *GPS Solut* 22(2):1–10. <https://doi.org/10.1007/s10291-018-0699-9>

Publisher's Note Springer Nature remains neutral with regard to jurisdictional claims in published maps and institutional affiliations.

Springer Nature or its licensor (e.g. a society or other partner) holds exclusive rights to this article under a publishing agreement with the author(s) or other rightsholder(s); author self-archiving of the accepted manuscript version of this article is solely governed by the terms of such publishing agreement and applicable law.



Qile Zhao is a professor at the GNSS Research Center of Wuhan University. He received his Ph.D. degree at Wuhan University in 2004. In 2006–2007, as a postdoctoral fellow, he performed research in DEOS, Delft University of Technology, the Netherlands. His current research interests are precise orbit determination of GNSS and low earth orbit satellites and high-precision positioning using GPS, Galileo and BDS.



Wenfei Guo is a teacher in GNSS Research Center, Wuhan University. He received his Ph.D. in Communication and Information Systems from Wuhan University in 2011. His research currently focuses on GNSS receivers and signal processing technologies, such as highly precise timing receivers, GNSS-R receivers, and anti-jamming receivers.



Jingyu Guo is a Master's Student at GNSS Research Center, Wuhan University. He received his Bachelor's degree at the School of Navigation Engineering at Wuhan University in 2016. His current research mainly focuses on PPP time transfer.



Shengfeng Gu received his Ph.D. from the GNSS Research Center of Wuhan University and is currently a postdoctoral researcher at Wuhan University. His current research mainly focuses on multi-GNSS data processing, PPP-RTK, and real-time ionosphere modeling.



Hongming Zuo is currently a master's student at GNSS Research Center, Wuhan University. His current research interests mainly focus on PPP timing and receiver clock modeling.



Xiaopeng Gong is currently a Ph.D. candidate at the GNSS Research Center, Wuhan University. He received his B.Sc. degree in 2013 from ChangAn University. His current research interests mainly focus on multi-system RTK and GNSS network solutions.